



CHORUS

This is the accepted manuscript made available via CHORUS. The article has been published as:

Three-nucleon interaction in heavy-ion collisions at intermediate energies

R. Wada

Phys. Rev. C **96**, 031601 — Published 5 September 2017

DOI: [10.1103/PhysRevC.96.031601](https://doi.org/10.1103/PhysRevC.96.031601)

Three nucleon interaction in Heavy ion collisions at intermediate energies

R. Wada^{1,*}

¹*Cyclotron Institute, Texas A&M University, College Station, Texas 77843*

(Dated: August 24, 2017)

The effect of a 3 nucleon (3N) interaction is studied for the production of high energy protons in heavy ion collisions in the incident energy range of 44A to 400A MeV. The 3N interaction is incorporated into the AMD transport model of Ono et al. as a 3N collision term, following a diagram of three consecutive binary collisions. For the theoretical $^{40}\text{Ar}+^{51}\text{V}$ reaction studies, no contribution from the 3N collisions is observed for high energy proton production at the incident energy of 44A MeV. However when the incident energy increases, the contribution increases gradually. At 200A MeV and above, the contribution is observed as distinct harder energy slopes in the proton energy spectra. The model is applied to the available Bevalac data for $^{40}\text{Ar}+^{40}\text{Ca}$ at 42A, 92A and 137A MeV. The experimental proton energy spectra are reasonably well reproduced at angles $\theta \geq 70^\circ$ for all three incident energies, showing negligible 3N contributions at 42A MeV and significant contributions at 137A MeV at the large laboratory angles. Good agreement at these large angles, where the 3N collision is a major mechanism to produce such protons, strongly indicates for the first time the importance of the 3N interaction in intermediate heavy ion reactions in a full transport calculation. The possible relation between the 3N collision term and the short range and the tensor interactions, is suggested.

PACS numbers: 25.70.Pq

Keywords: Intermediate Heavy ion reactions, three nucleon collision, antisymmetrized molecular dynamics

In recent intensive explorations of nuclear research, three-nucleon (3N) force problems have become one of the frontier researches [1]. In nuclear matter, the 3N force plays a vital role in nuclear structure, nuclear reactions, and nuclear astrophysics. Examples are studies in *ab initio* calculations for light and magic nuclei [3, 4], nuclear drip lines [5, 6], properties of the nuclear equation of state [7–9], neutron skins [10] and neutron stars [11–13]. Deeper understanding of 3N forces will open up new insights not only in nuclear physics, but also in related areas, such as astrophysics.

The study of 3N forces began as early as the 1950's. Fujita and Miyazawa introduced a three-body interaction [14]. However 3N forces are highlighted by the recent microscopic *ab initio* nuclear structure calculations [15, 16]. A variety of different models have been proposed [17–21]. A common feature of these calculations is to use realistic nucleon-nucleon (2N) and 3N forces. These studies have unambiguously shown that 3N forces improve significantly the reproduction of the energy levels of light nuclei.

The 3N force consists of two parts, an attractive part and a repulsive part [22, 23]. The attractive part is typically expressed by two-pion exchange with excitation of an intermediate Δ resonance following the Fujita-Miyazawa diagram and is important at normal and sub-normal density, and thus for structural calculations. For nuclear reaction studies, the repulsive part becomes important when the nuclear density exceeds the normal nuclear density [22]. In Refs. [24–26], Furumoto et al.

used complex G-matrix interactions including the effect of phenomenological 3N repulsive forces based on the extended soft core model of Rijken [27], in a folding-model calculation. They applied their model to nucleus-nucleus elastic scattering in the incident energy range of 70A to 400A MeV [25, 26] and showed that the repulsive nature of the 3N forces at these incident energies changes the diffraction pattern of the elastic scattering, caused by the interference between near and far side of the elastic scattering, and provided an observable for the 3N force as a direct probe in nuclear scattering experiments. Recently Qu et al. performed a high resolution measurement of the $^{12}\text{C}+^{12}\text{C}$ elastic and inelastic scattering at 100A MeV, using the Grand Raiden magnetic spectrometer at RCNP (Research Center of Nuclear Study) in Japan, and successfully demonstrated the repulsive effect of the 3N forces [28, 29].

In addition to the above reaction studies, other reaction studies have been performed in which a 3N collision term is used. In the model, the 3N collision term has only one free parameter, *i.e.*, the 3N collision cross section. The importance of the 3N collision term at intermediate heavy ion collisions was first pointed out by Mr̄owczyński [30]. Bonasera et al. studied it in detail and put it into a transport model formalism [31–33].

Experimentally Germain et al. performed $^{36}\text{Ar}+^{181}\text{Ta}$ collisions at 94A MeV and measured high energy protons, for which proton energy often exceeds 3-4 times the incident energy per nucleon [36]. They compared the experimentally observed high energy proton spectra with those from Boltzmann-Nordheim-Vlasov (BNV) transport simulations. Since they were not able to reproduce the slope and amplitude of the high energy proton spectra without adding a 3N collision term, they concluded

*E-mail at:wada@comp.tamu.edu

that the 3N collision term takes a crucial role in the production of the high energy protons at this energy. However their conclusion was based on a perturbed method of BNV calculations with a sharp cut-off of the Fermi momentum in initial nuclei. Therefore in their calculation the high momentum tail of Fermi motion in hot nuclear matter is not taken into account properly in the collision process.

In our recent study [37], we demonstrated that a careful treatment of the Fermi motion in a transport model, especially for the high momentum distribution in hot nuclear matter, is crucial for the production of high energy protons. The calculations are based on an antisymmetrized molecular dynamics (AMD) [38]. In the extended AMD [39, 40], the Fermi motion is taken into account as a quantum fluctuation, a quantum branching of the wave packets called a diffusion process in the nucleon propagation in a mean field. In our work in Ref. [37], we also take into account the quantum fluctuation in each collision process and the modified code is called AMD-FM. These treatments are quite different from that in most other transport models, in which the Fermi motion is added to nucleons only once in the initial nuclei, whereas in AMD-FM, a new Fermi motion is assigned as a momentum fluctuation in the diffusion process and each collision, thus many times throughout the calculation. The AMD-FM significantly improves the reproduction of the high energy protons in available experimental data of $^{40}\text{Ar} + ^{51}\text{V}$ at 44 MeV/nucleon [41] and $^{36}\text{Ar} + ^{181}\text{Ta}$ at 94 MeV/nucleon [36]. I extend this study to include a 3N collision term at higher incident energies in this article.

According to Ref. [30], the ratio of the number of 2N (N_2) and 3N (N_3) collisions for a gas in equilibrium is given as

$$\frac{N_3}{N_2} = \frac{4}{3\sqrt{\pi}}\sigma^{3/2}\rho, \quad (1)$$

where σ is the 2N collision cross section and ρ is the nuclear matter density. Thus the number of 3N collisions increases as the nuclear density increases relative to that of 2N collisions. In the central collisions of intermediate heavy ion reactions, the density of nuclear matter increases in the overlap region [42]. The maximum density at the center of the overlap region reaches $\sim 2\rho_0$ for $^{40}\text{Ca} + ^{40}\text{Ca}$ at 400 MeV/nucleon where ρ_0 is the normal nuclear matter density. In 3N collisions, one of three nucleons can have a large kinetic energy in their center of mass system, compared to that of 2N collisions, and therefore 3N collisions may significantly contribute to the high energy proton production in the energy range above 100 MeV/nucleon.

Short range correlations (SRC) are another mechanism to generate high energy protons [48, 49]. Recent high momentum transfer measurements [50–55] have shown that nucleons in nuclear ground states can form pairs with large relative momentum and small center-of-mass momentum due to the short-range correlation of the

nucleon-nucleon interaction (2N-SRC). Detailed experimental studies indicate that these pairs are preferentially formed between proton and neutron, because of the nature of the tensor force in the 2N interaction. When these pairs are knocked out by large momentum transfer reactions, such as $(e, e'pn)$ or (p, ppn) , high energy nucleons are emitted in a back to back configuration in their center of mass system. However in order to knock out these pairs, a few to several GeV electron or proton beams have been used. In the incident energy range of heavy ion collisions between $44A \text{ MeV}$ and $400A \text{ MeV}$, described in the present work, I expect that the 2N-SRC contribution by the knockout pair process for the high energy proton production is small and focus instead on the 3N collision term. However SRC certainly contributes to the high momentum tail of the Fermi distribution which is crucial for the high energy proton production described in Ref. [37].

The upper limit of the incident energy ($400A \text{ MeV}$) in this study is set from the AMD code, in which meson productions are not taken into account. This upper energy also limits other meson exchange processes as a source for the high energy proton production in simulations.

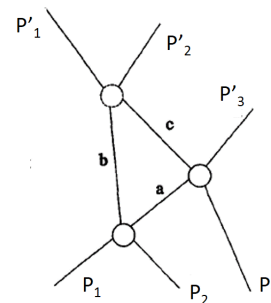


FIG. 1: Diagrammatic representation of 3N collision. The lines indicate particle trajectories and the meeting points indicate the location of the particles at the time of collision. P_1, P_2, P_3 represent the initial states and P'_1, P'_2, P'_3 are the final states. **a**, **b**, **c**, are intermediate states treated as virtual states in the 3N collision process.

It is natural for the 3N collision term to relate to the 3N forces, since the 3N collision term is, as shown below, essential for the high energy proton production at intermediate heavy ion collisions. As mentioned earlier, it has become clear for light nuclei that one of the 3N forces has to be introduced for a satisfactory description of finite-mass nuclei. 2N interactions are known to have a strong repulsion at short distance in addition to a strong tensor force at long and intermediate ranges [43, 44]. These two characteristics of the 2N interactions provide the high momentum components of nucleon motion in nuclear matter. The tensor force produces the characteristic D-wave state of a nucleon pair, which comes from the strong SD coupling of the tensor force. This D-wave state is spatially compact as compared with the S-wave state due to the high-momentum component of the tensor

correlation. The 3N interaction can be described by the successive of these two interactions, where the intermediate states are treated as virtual states. Therefore the high momentum component can be emphasized without constraints in a three nucleon correlation. In a recent study of Myo et al. [45], they incorporate the tensor and short range interactions naturally into a 3N force in the AMD formalism in the tensor-optimized AMD (TOAMD) for structure calculations. However no attempt has been made to describe the 3N collision term from a microscopic 3N force yet. The following 3N collision treatment is an attempt to include the microscopic 3N forces phenomenologically as a 3N collision term through the high momentum component of the Fermi motion and applies it in intermediate heavy ion collisions.

A 3N collision term is incorporated into AMD-FM following the description in Ref. [33]. I will refer this version as AMD-FM(3N). The 3N interaction is simply calculated by a succession of three binary collisions where one pair of nucleons interacts twice when three nucleons are in the collision distance each other as shown diagrammatically in Fig. 1. As demonstrated by Germain et al. in Ref. [36], a 3N collision term enhances the high energy proton production. This is simply because in the 3N collision process, kinetic energy of three nucleons can be shared between them under less restrictions of the momentum and energy conservation. This makes one of nucleons can have higher energy than those in 2N collision processes, because the third nucleon in a 3N collision can provide additional kinetic energy available. Therefore the high energy proton emission mechanism in the 3N collision term is purely kinematical in the present calculation. Another difference between the 3N collision term incorporated into AMD-FM(3N) and three of binary collisions is that in the 3N collision process, intermediate state, **a**, **b**, **c** in the diagram, are treated as virtual states and only final states, P'_1 , P'_2 , and P'_3 , are required to satisfy the Pauli exclusion principle and energy+momentum conservations, whereas in the simple three binary collisions, all 2N final states are examined for the Pauli exclusion principles and the conservation laws. A virtual state meant here is that, it is a state when the system might violate conservation laws and Pauli principle for a short time which is connected to the Heisenberg principle. For instance the energy can be violated up to ΔE in a time $\hbar/\Delta E$. Similarly for momentum. Pauli blocking violation is essentially from the energy conservation.

In each collision in the diagram, the same treatment as in Ref. [37] is made for each nucleon momentum to take into account the Fermi momentum distribution as a Gaussian distribution and to avoid double counting with the diffusion process. The effect is called "Fermi boost". The treatment of the intermediate states, **a**, **b**, **c**, as virtual states in the 3N collision process, can enhance the role of the high momentum component of the Fermi momentum distribution in the production of high energy protons, as shown below.

After collisions are Pauli-allowed in a given time span,

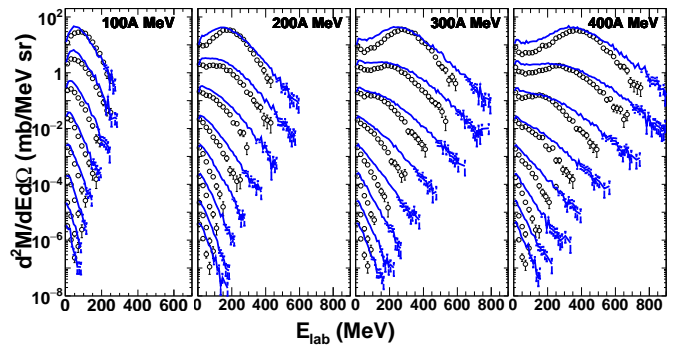


FIG. 2: (color online) Simulated results of proton energy distributions for $^{40}\text{Ar} + ^{51}\text{V}$ at different incident energies. Histograms represent the results of AMD-FM(3N) and circles are from AMD-FM. The spectra in each column are plotted every 20° from $\theta = 10^\circ$ at the top to $\theta = 170^\circ$ at the bottom. Each spectrum is multiplied by a factor of 10 from the bottom to avoid overlap each other. The incident energy is 100A MeV on the left to 400A MeV on the right, indicating on the top.

momentum and energy are restored in the same way as described in Ref. [37]. The same Gogny interaction [46] and the Li-Machleidt NN cross section [47] are used. 3N collisions are attempted in a similar criteria as that of 2N collisions between 3 pair of nucleons. For the 3N collisions, however, the collision cross section is treated as a constant free parameter. When all relative distances of the 3 pairs of nucleons are within a collision distance $r = \sqrt{\sigma/\pi}$, a 3N collision is attempted. A constant value of 40mb is used for σ in the following calculations.

The calculated results of AMD-FM (circles) and AMD-FM(3N) (histograms) are compared in Fig. 2 for the $^{40}\text{Ar} + ^{51}\text{V}$ reactions at 100, 200, 300 and 400A MeV. At 100A MeV on the left, the energy spectra are very similar at different angles between two calculations, but the yields of AMD-FM(3N) are slightly larger, by a factor of 2 at most. When the incident energy increases to 200A MeV, the shapes of the energy spectra show a distinct difference, that is, the energy slopes of AMD-FM(3N) show much harder slopes than those of AMD-FM. Similar differences are also observed at higher incident energies. One should note that the slope of the spectra barely depend on the impact parameter range, because they originate essentially from the 2N or 3N collisions. One can also see broader peaks at the lower proton energy in the forward spectra for the AMD-FM(3N) simulations. This can be explained as follows: At the low energy side, the spectra of AMD-FM show a semi-Gaussian distribution. The contribution from the 3N collisions also becomes a Gaussian distribution, because of the Fermi boost for the third nucleon, and thus they are overlaid on top of each other, which causes a broadening of the distribution. On the high energy side, on the other hand, the spectra of AMD-FM show an exponential fall off and the 3N contribution becomes visible only in the higher energy side.

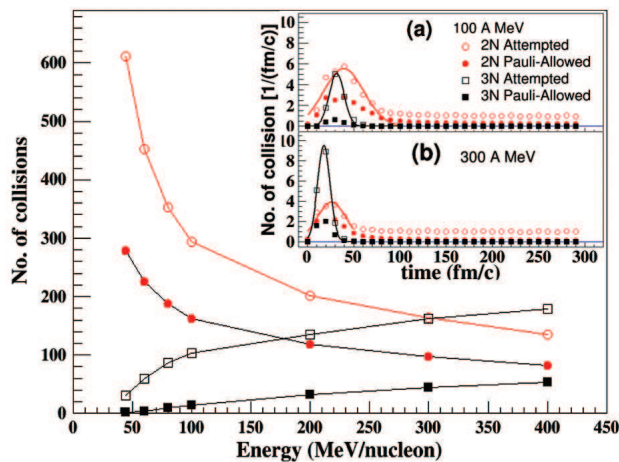


FIG. 3: (color online) Summed number of 2 body (circles) and 3 body (squares) collisions are plotted as a function of incident energy. Insert: Number of 2N and 3N collisions are plotted as a function of reaction time. (a) $^{40}\text{Ar} + ^{51}\text{V}$ at $100A \text{ MeV}$. The density in the overlap region becomes maximum at $\sim 30 \text{ fm/c}$ at this energy. (b) $^{40}\text{Ar} + ^{51}\text{V}$ at $300A \text{ MeV}$. The density becomes maximum at $\sim 20 \text{ fm/c}$ at this energy. The sigma of the Gaussians are 21.7 (15.9) for 2N and 8.0 (6.8) for 3N attempted collisions at $100A(300A) \text{ MeV}$, respectively.

In the insert of Fig. 3, the number of collisions is plotted as a function of reaction time for attempted collisions and Pauli-allowed collisions at $100A \text{ MeV}$ in (a) and $300A \text{ MeV}$ in (b). At both energies, the maximum number of collisions per time occurs at the time of overlap between the projectile and target. Around this time period, the shape of the collision distributions are very similar between attempted and Pauli-allowed collisions. When the peaks are fit by a Gaussian distribution, the width for the 3N collisions is less than half of that of the 2N collisions, indicating that the 3N collisions are more localized in time, at the time of the maximum density. This is what is expected from Eq. (1). This width difference in the numbers between the 2N and 3N collisions indicates how quickly the overlap region expands in time.

In Fig. 3 a summary of the number of collisions is plotted as a function of the incident energy. The number of collisions is calculated around the peak, using a Gaussian fit as shown in the insert. Collisions at later stages are not included. The number of the 2N collisions decreases rapidly as the incident energy increases from $44A$ to $100A \text{ MeV}$, whereas the number of the 3N attempted collisions increases rapidly in this energy range. The number of the Pauli-allowed 3N collisions below $60A \text{ MeV}$ is small and increases very slowly. At $100A \text{ MeV}$, about 50% of the attempted 2N collisions are blocked by the Pauli exclusion principle. The blocking is more significant for the 3N collisions, where nearly 90% of the collisions are blocked. At $300A \text{ MeV}$, about 40% of the 2N collisions are Pauli-blocked, whereas for the 3N collisions about 75% are blocked. These numbers of blocking indicate that, even above $100A \text{ MeV}$, a careful

treatment of the Pauli blocking is still very important, especially for the 3N collisions.

Proton energy spectra in intermediate and relativistic heavy ion collisions were studied extensively in late 1970's and 1980's at the Bevalac in the Lawrence Berkeley Laboratory. Many experiments were performed, using a variety of beams and targets at the incident energy range of $42A \text{ MeV}$ to $2.1A \text{ GeV}$ [56–59]. In order to verify the contribution of the 3N collisions, the incident energy range of $50A$ to $200A \text{ MeV}$ is desirable, since in this energy range, the contribution of the 3N collisions in the high energy proton spectra starts to appear and shows a significant increase, according to the simulations shown in Fig. 2. From the AMD simulation point of view, lighter reaction systems are preferable, since the AMD code is a very cpu time demanding program and the required cpu time increases approximately in proportion to A^3 where A is the system size. Under these conditions, the AMD-FM(3N) is applied to proton energy spectra in the $^{40}\text{Ar} + ^{40}\text{Ca}$ reaction at $42, 92A$ and $137A \text{ MeV}$ [60, 61] and $^{40}\text{Ar} + ^{51}\text{V}$ at $44A \text{ MeV}$ [41]. In Fig. 4(a) to (c), simulated results are shown with the Bevalac data. One should note that, according to Ref. [60], the normalization for the $42A \text{ MeV}$ data suffered some problem in the beam monitoring detectors. Therefore in the figure, the experimental data are normalized to the AMD simulations at backward angles, by multiplying by a factor of 0.2. All other results are given in an absolute scale. For the simulations, the impact parameter range of $0\text{-}8 \text{ fm}$ is used, whereas the experimental data are inclusive. In general, the simulated spectra with AMD-FM and AMD-FM(3N) are almost identical at $42A \text{ MeV}$ and one can start to see noticeable differences between calculated spectra (solid and dashed curves) at $92A \text{ MeV}$ and the difference increases at $137A \text{ MeV}$. The experimental differential cross sections and slopes of proton energy spectra are well reproduced by the AMD-FM(3N) simulations at $\theta_{lab} \geq 70^\circ$ for three incident energies. The experimental data are poorly reproduced by AMD-FM without the 3N collision term at $92A$ and $137A \text{ MeV}$ at all angles. The experimental spectra at forward two angles at $42A \text{ MeV}$ are significantly under-predicted even with AMD-FM(3N). However these large discrepancies are not observed in the previous study for a similar reaction of $^{40}\text{Ar} + ^{51}\text{V}$ at $44A \text{ MeV}$ in Ref. [37]. The calculated results are also shown in Fig. 4(d). The experimental data were taken at the Grand Accélérateur National d'Ions Lourds (GANIL), France, using a large BaF_2 array, MEDIA detector [64]. The observed proton energy spectra are well reproduced at all angles both for the AMD-FM and AMD-FM(3N) calculations when the impact parameter range of $0 < b \leq 6 \text{ fm}$ is used. For the same impact parameter range of $0 < b \leq 8 \text{ fm}$ as that used for $^{40}\text{Ar} + ^{51}\text{V}$ at $44A \text{ MeV}$, the experimental yields are overpredicted by a factor of 1.6, but the spectral shapes stay very similar. In order to verify these discrepancies, further experimental studies, especially exclusive measurements, are needed.

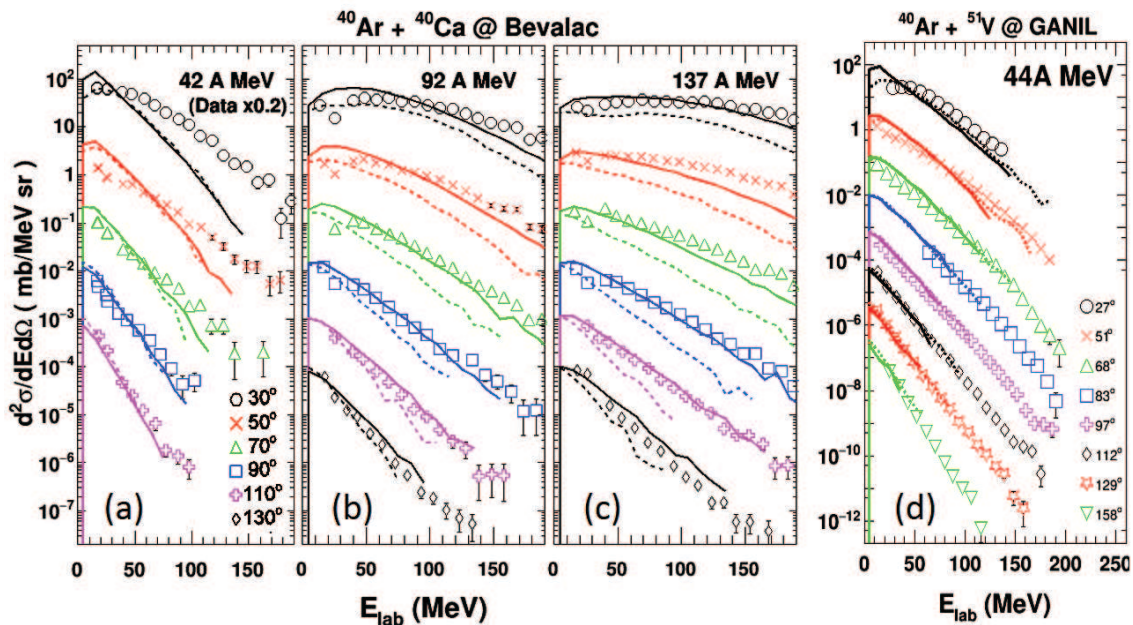


FIG. 4: (color online) Simulated results of proton energy spectra for the $^{40}\text{Ar} + ^{40}\text{Ca}$ reactions at 42A(a), 92A (b) and 137A MeV (c), and for the $^{40}\text{Ar} + ^{51}\text{V}$ reactions at 44A MeV in (d). Data in (a) to (c) are taken from Ref. [60] and (d) are from Ref. [41]. Solid curves are for the results of AMD-FM(3N) and dashed curves are for those of AMD-FM. Data and results are plotted in an absolute scale. All results are multiplied by a factor of 10^{-n} ($n = 0$ to 5 in (a) to (c) and 8 in (d)) from top to bottom for clarity. The data at 42A MeV in (a) are multiplied by a factor of 0.2. See details in the text.

In summary, a 3N interaction is incorporated as a 3N collision term into AMD-FM. The quantum fluctuation in momentum space is taken into account in each collision process and the new code is called AMD-FM(3N). The contribution of the 3N collisions is theoretically investigated for high energy proton production in the $^{40}\text{Ar} + ^{51}\text{V}$ reaction at 44A to 400A MeV. At 44A MeV, no noticeable contribution is observed and it becomes notable at 100A MeV and a significant increase is observed as the energy increases to 200A MeV. In order to verify the importance of the 3N interaction in heavy ion collisions in experiments, AMD-FM(3N) is applied to the available Bevalac data of the $^{40}\text{Ar} + ^{40}\text{Ca}$ reaction at 42A, 92A and 137A MeV in Refs. [60, 61]. The experimental proton energy spectra at $\theta \geq 70^\circ$ are reproduced reasonably well at the observed energy range by the AMD-FM(3N) at all three incident energies. Good agreement between the experimental data and AMD-FM(3N) simulations indicates for the first time the importance of the 3N interaction in

intermediate heavy ion reactions in a full transport simulation. Even though the origin of the 3N collision term has not yet been related to the microscopic 3N forces, the enhancement of the proton spectra at high energy suggests that they may originate from the short range correlation and the tensor force at intermediate and long range into the high energy tail of the Fermi motion in hot nuclear matter.

Acknowledgments

I would like to thank Dr. A. Ono for providing me his AMD code and Dr. A. Bonasera for helpful discussions about the three body collision process. I also thank Dr. H. Toki and Dr. H. Horiuchi at RCNP for their helpful comments and Dr. J. B. Natowitz for his careful reading of the manuscript, helpful comments and his encouragements. This work is supported by the US Department of Energy under Grant No. DE-FG02-93ER40773.

[1] H.-W. Hammer, A. Nogga, A. Schwenk, Rev. Mod. Phys. 85, 197 (2013).
 [2] B. Friman and A. Schwenk, arXiv:1101.4858v1.2011
 [3] J. E. Lynn, J. Carlson, E. Epelbaum, S. Gandolfi, A. Gezerlis, and A. Schwenk, Phys. Rev. Lett. 113, 192501 (2014).
 [4] K. Sieja and F. Nowacki, Phys. Rev. C 85, 051301(R) (2012).

[5] Takaharu Otsuka, Toshio Suzuki, Jason D. Holt, Achim Schwenk, and Yoshinori Akaishi, Phys. Rev. Lett. 105, 032501 (2010).
 [6] J. D. Holt, J. Menendez, and A. Schwenk, Phys. Rev. Lett. 110, 022502 (2013).
 [7] W. Zuo, Z. H. Li, A. Li, and G. C. Lu, Phys. Rev. C 69, 064001 (2004).
 [8] M. Baldo and Alaa Eldeen Shaban, Phys. Lett. B 661,

- 373 (2008).
- [9] Peng Yin, Jian-Yang Li, Pei Wang, and Wei Zuo, *Phys. Rev. C* **87**, 014314 (2013).
- [10] M. B. Tsang, J. R. Stone, F. Camera, P. Danielewicz, S. Gandolfi et al., *Phys. Rev. C* **86**, 015803 (2012).
- [11] X. R. Zhou, G. F. Burgio, U. Lombardo, H.-J. Schulze, and W. Zuo, *Phys. Rev. C* **69**, 018801 (2004).
- [12] D. Davesne, J. W. Holt, A. Pastore, and J. Navarro, *Phys. Rev. C* **91**, 014323 (2015).
- [13] S. Goudarzi and H. R. Moshfegh, *Phys. Rev. C* **91**, 054320 (2015).
- [14] J. Fujita and H. Miyazawa, *Prog. Theor. Phys.* **17**, 360 (1957).
- [15] J. Carlson, S. Gandolfi, F. Pederiva, S. C. Pieper, R. Schiavilla, K. E. Schmidt, and R. B. Wiringa, *Rev. Mod. Phys.* **87**, 1067 (2015).
- [16] E. Epelbaum, H.-W. Hammer, Ulf-G., Meißner, *Rev. Mod. Phys.* **81**, 1773 (2009).
- [17] R. Roth, J. Langhammer, A. Calci, S. Binder, and P. Navratil, *Phys. Rev. Lett.* **107**, 072501 (2011).
- [18] H. Hergert, S. K. Bogner, S. Binder, A. Calci, J. Langhammer, R. Roth, and A. Schwenk, *Phys. Rev. C* **87**, 034307 (2013).
- [19] T. A. Löhde, E. Epelbaum, H. Krebs, D. Lee, U.-G. Meiner, and G. Rupak, *Phys. Lett. B* **732**, 110 (2014).
- [20] J. Simonis, K. Hebeler, J. D. Holt, J. Menendez, and A. Schwenk, *Phys. Rev. C* **93**, 011302 (2016).
- [21] G. Hagen, A. Ekström, C. Forssén, G. R. Jansen, W. Nazarewicz et al., *Nature Physics* **12**, 186 (2016).
- [22] R. B. Wiringa, V. Fiks and A. Fabrocini, *Phys. Rev. C* **38**, 1010 (1988).
- [23] Steven C. Pieper, V. R. Pandharipande, R. B. Wiringa, and J. Carlson, *Phys. Rev. C* **64**, 014001 (2001).
- [24] T. Furumoto, Y. Sakuragi, and Y. Yamamoto, *Phys. Rev. C* **78**, 044610 (2008).
- [25] T. Furumoto, Y. Sakuragi, and Y. Yamamoto, *Phys. Rev. C* **79**, 011601(R) (2009).
- [26] T. Furumoto, Y. Sakuragi, and Y. Yamamoto, *Phys. Rev. C* **82**, 044612 (2010).
- [27] T. A. Rijken, *Phys. Rev. C* **73**, 044007 (2006).
- [28] W. W. Qu, G. L. Zhang, S. Terashima, T. Furumoto, Y. Ayyad et al., *Phys. Lett. B* **751**, 1 (2015).
- [29] W. W. Qu, G. L. Zhang, S. Terashima, T. Furumoto, Y. Ayyad et al., *Phys. Rev. C* **95**, 044616, (2017).
- [30] St. Mrówczyński, *Phys. Rev. C* **32**, 1784 (1985)
- [31] A. Bonasera a and F. Gulminelli, *Phys. Lett. B* **259**, 399 (1991).
- [32] A. Bonasera a,b and F. Gulminelli, *Phys. Lett. B* **275**, 24 (1992).
- [33] A. Bonasera a,b and F. Gulminelli, *J. Mollitorisc*, *Phys. Rep.* **243**, 1 (1994)
- [34] R. Brockmann and R. Machleidt, *Phys. Rev. C* **42**, 1965 (1990).
- [35] G. Q. Li, R. Machleidt, and R. Brockmann, *Phys. Rev. C* **45**, 2782 (1992).
- [36] M. Germain, Eudes, E. Guilbault, P. Lautridou, J.L. Laville et al., *Nucl. Phys. A* **620**, 81 (1997).
- [37] W. Lin, X. Liu, R. Wada, M. Huang, P. Ren et al., *Phys. Rev. C* **94**, 064609 (2016).
- [38] Akira Ono, Hisashi Horiuchi, Toshiki Maruyama and Akira Ohnishi, *Prog. Theo. Phys.* **87**, 1185 (1992).
- [39] A. Ono, *Phys. Rev. C* **53**, 2958 (1996).
- [40] A. Ono, *Phys. Rev. C* **59**, 853 (1999).
- [41] R. Coniglione, P. Sapienza, E. Migneco, C. Agodi, R. Alba et al., *Phys. Lett. B* **471**, 339 (2000).
- [42] X. Liu, W. Lin, M. Huang, R. Wada, J. Wang et al., *Phys. Rev. C* **92**, 014623 (2015).
- [43] S. C. Pieper and R. B. Wiringa, *Annu. Rev. Nucl. Part. Sci.* **51**, 53 (2001).
- [44] R. B. Wiringa, R. A. Smith, and T. L. Ainsworth, *Phys. Rev. C* **29**, 1207 (1984).
- [45] Takayuki Myo, Hiroshi Toki, Kiyomi Ikeda, Hisashi Horiuchi, and Tadahiro Suhara, *Prog. Theor. Exp. Phys.* **073D02** (2015).
- [46] J. Dechargé and D. Gogny, *Phys. Rev. C* **21**, 1568 (1980).
- [47] G. Q. Li and R. Machleidt, *Phys. Rev. C* **48**, 1702 (1993); **49**, 566 (1994).
- [48] O. Hen, M. Sargsian, L. B. Weinstein, E. Piasetzky, H. Hakobyan et al., *Science* **346**, 614 (2014)
- [49] R. Subedi, R. Shneor, P. Monaghan, B. D. Anderson, K. Aniol et al., *Science* **320**, 1476 (2008)
- [50] E. Piasetzky, M. Sargsian, L. Frankfurt, M. Strikman, and J. W. Watson, *Phys. Rev. Lett.* **97**, 162504 (2006).
- [51] R. A. Niyazov, L. B. Weinstein, G. Adams, P. Ambrozewicz, E. Anciant et al. (CLAS Collaboration), *Phys. Rev. Lett.* **92**, 052303 (2004).
- [52] K. Sh. Egiyan, N. Dashyan, M. Sargsian, S. Stepanyan, L. B. Weinstein et al. (CLAS Collaboration), *Phys. Rev. C* **68**, 014313 (2003).
- [53] K. S. Egiyan, N. B. Dashyan, M. M. Sargsian, M. I. Strikman, L. B. Weinstein et al., *Phys. Rev. Lett.* **96**, 082501 (2006).
- [54] J. Aclander, J. Alster, D. Barton, G. Bunce, A. Carroll et al., *Phys. Lett. B* **453**, 211 (1999).
- [55] A. Tang, J. W. Watson, J. Aclander, J. Alster, G. Asryan et al., *Phys. Rev. Lett.* **90**, 042301 (2003).
- [56] J. Gosset, H. H. Gutbrod, W. G. Meyer, A. M. Poskanzer, A. Sandoval, R. Stock, and G. D. Westfall, *Phys. Rev. C* **16**, 629 (1977).
- [57] A. Sandoval, H. H. Gutbrod, W. G. Meyer, R. Stock, Ch. Lukner et al., *Phys. Rev. C* **21**, 1321 (1980).
- [58] R. A. Cecil, B. D. Anderson, A. R. Baldwin, R. Madey, W. Schimmerling, J. W. Kast, and D. Ortendahl, *Phys. Rev. C* **24**, 2013 (1981).
- [59] B. V. Jacak, G. D. Westfall, C. K. Gelbke, L. H. Harwood, W. G. Lynch, D. K. Scott, H. Stcker, M. B. Tsang, and T. J. M. Symons, *Phys. Rev. Lett.* **51**, 1846 (1983).
- [60] H. Kruse, B. V. Jacak, J. J. Molitoris, G. D. Westfall, and H. Stcker, *Phys. Rev. C* **31**, 1770 (1985).
- [61] B. V. Jacak, G. D. Westfall, G. M. Crawley, D. Fox, C. K. Gelbke et al., *Phys. Rev. C* **35**, 1751 (1987).
- [62] R. Wada, K. Hagel, J. Cibor, M. Gonin, Th. Keutgen et al., *Phys. Rev. C* **62**, 034601 (2000).
- [63] G. Tian, R. Wada, Z. Chen, R. Han, W. Lin et al., *Phys. Rev. C* **95**, 044613 (2017).
- [64] E. Migneco, C. Agodi, R. Alba, G. Bellia, R. Coniglione et al., *Nucl. Inst. Meth. A* **314**, 31 (1992).